Probing Excited-State Dynamics and Intramolecular Proton Transfer in 1-Acylaminoanthraquinones via the Intermolecular Solvent Response

Sarah J. Schmidtke, David F. Underwood, and David A. Blank*

Department of Chemistry, University of Minnesota, 207 Pleasant Street SE, Minneapolis, Minnesota 55455

Received: April 15, 2005; In Final Form: June 13, 2005

The dynamics of a series of 1-acylaminoanthraquinones with varying degrees of excited-state intramolecular proton transfer are studied in acetonitrile and dichloromethane. Events are followed via changes in the third-order intermolecular Raman response as a function of time after resonant excitation of the chromophore. Compared to electronically resonant probes of the solute, measuring the ultrafast dynamics using the nonresonant solvent response offers a new and complementary perspective on the events that accompany excitation and proton transfer. Experimentally observed changes in the nuclear polarizability of the solvent follow dynamic changes in the solvent−solute interactions. Reorganization of the solvent in response to the significant changes in the intermolecular interactions upon proton transfer is found to play an important role in the reaction dynamics. With transfer of the proton taking place rapidly, the solvent controls the dynamics via the time-dependent evolution of the free energy surface, even on subpicosecond time scales. In addition, the solvent response probes the effects of intermolecular energy transfer as energy released during the reactive event is rapidly transferred to the local solvent environment and then dissipates to the bulk solvent on about a 10 ps time scale. A brief initial account of a portion of this work has appeared previously, *J. Am. Chem. Soc.* **2004**, *126,* 8620−8621.

1. Introduction

Excited-state intramolecular proton transfer (ESIPT) is important in a variety of organic and inorganic processes including photosynthesis, metabolism, and DNA base-pair tautomerization.[1−6] Compounds that undergo proton transfer in the condensed phase have been the subject of many experimental and computational studies.[5,7−28] Spectroscopic measurements of the dynamics in condensed phase systems have focused primarily on probing the electronic energy gap of the chromophore. These studies have provided a wealth of information concerning the time-dependent evolution of the reactant and product populations. However, following the dynamics via changes in the solute's optical transitions does present some significant challenges. Mapping the electronic energy gap onto the reaction coordinate can be very difficult because this requires detailed knowledge about both the ground and excited-state potential energy surfaces. For example, transition energies that are not unique to a single configuration of the system may arise, including overlapping transitions of the reactants and products. In addition, resonant solute probes provide limited information concerning the dynamic reorganization of the solvent that often plays an integral role in charge-transfer reactions. The solute's ability to report on the local solvent environment is typically compromised by large, rapid changes in the transition energy that accompany progress along the reaction coordinate(s). Conclusions concerning the participation of the solvent are restricted to inference based on the rate of solute transformation, and information concerning changes of the local solvent response both during and as a result of the reaction are typically absent. Our research group recently introduced a method to probe the time-dependent change in the nonresonant intermolecular solvent response following a photoinitiated event in solution.[29−31] Tracking the solvent response provides a new, complementary perspective and provides additional understanding of the complex dynamics in these condensed-phase reactions.

In this study, the nonresonant intermolecular response was probed following photoexcitation of a series of 1-acylaminoanthraquinones (AAQs) in acetonitrile and dichloromethane. These compounds offer a model system for ESIPT. It has been established previously that by varying the acyl substituent group of the AAQ, see Figure 1, the extent of ESIPT can be controlled. In an extensive investigation, Smith et al. reported that as the electrophilicity of the acyl substituent is increased the ESIPT ranges from essentially absent in 1-(heptanoylamino)anthraquinone, HPAQ, to nearly instantaneous in 1-(trifluoroacetylamino)-anthraquinone, TFAQ.[25,26] The static fluorescence spectrum for TFAQ indicates near complete proton transfer in all of the solvents investigated, and time-resolved measurements found that the product was created within the time resolution of the experiments, ca. 350 fs, suggesting a lack of solvent control.[25] Two compounds with acyl substituent electrophilicities that lie between TFAQ and HPAQ, 1-(dichloroacetylamino)anthraquinone, DCAQ, and 1-(chloroacetylamino)anthraquinone, CAAQ, represent intermediate cases in which the extent of ESIPT varies significantly depending on the solvent. Because the technique used in the present study probes time-dependent changes in the solvent response rather than a resonant transition of the reactants and products, the ability to tune the degree of proton transfer (PT) provides contrast between the dynamics associated with electronic excitation and proton transfer.

We refer to the molecule prior to PT as the normal form (N) and following PT as the tautomeric form (T), see Figure 1. The electronic ground and first excited singlet states of each are then labeled as $S_0(N)$, $S_0(T)$, $S_1(N)$, and $S_1(T)$. In the electronic ground state, the normal form is thermodynamically favored

* Corresponding author. E-mail: blank@chem.umn.edu. Phone: (612) 624-0571. Fax: (612) 624-1589.

10.1021/jp051964l CCC: $30.25
Published on Web 07/21/2005

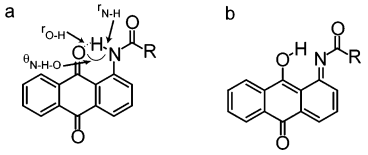

Figure 1. Structures of normal (a) and tautomeric (b) 1-(acetylamino)-anthraquinones. R═$(CH_2)_5CH_3$ (HPAQ), R═CH_2Cl (CAAQ), R═$CHCl_2$ (DCAQ), R═CF_3 (TFAQ).

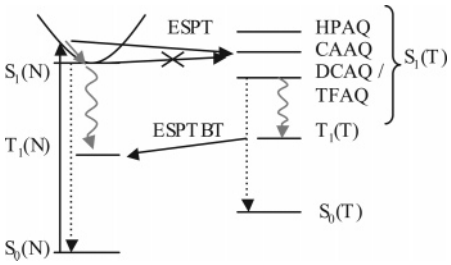

Figure 2. Schematic of energy levels for the ground and excited states of the normal and tautomeric forms of the AAQs. The states are labeled for the normal (N) and tautomeric (T) forms in the singlet (S) and triplet (T) states.

and effectively the only form prior to photoexcitation at room temperature. In the S_1 state, the N and T forms are energetically similar and ESIPT varies from endothermic to exothermic depending on the acyl substituent. Using the ratio of static fluorescence from $S_1(N)$ and $S_1(T)$ in cyclohexane, we can roughly approximate the free energy difference in the excited state to range from 0.6 kcal/mol for HPAQ to −2 kcal/mol for TFAQ.[25] An energy level diagram is shown in Figure 2. Previous investigations of selected AAQs have indicated that increases in the solvent polarity stabilize $S_1(N)$ to a greater extent than $S_1(T)$.[25−27] In the intermediate case of CAAQ, the change in solvent from acetonitrile to cyclohexane results in exchange of the dominant fluorescent species from the normal form to the proton-transfer tautomer.[25] Time-resolved fluorescence for CAAQ in acetone indicated a delayed rise in the appearance of $S_1(N)$ emission concurrent with decay in $S_1(T)$ emission. Within the uncertainty in the measured time scales, this was tentatively assigned as the result of differential solvation between $S_1(T)$ and $S_1(N)$. Using pump−probe spectroscopy with ca. 100 fs time resolution, Neuwahl et al. demonstrated a delay in the appearance of $S_1(T)$ in both acetonitrile and dichloromethane.[27] In this study, the authors explained the delayed rise of the tautomeric form in terms of kinetics establishing equilibrium across a potential energy barrier along the proton-transfer (PT) coordinate.

The experimental results we present here use a technique developed in our laboratory, resonant pump third-order Raman probe spectroscopy (RaPTORS).[29,30] This technique directly probes the nuclear polarizability of the solvent following excitation of a chromophore. The result is a measurement of changes in the local intermolecular solvent response during a reactive event in solution. We recently reported initial RaPTORS measurements of CAAQ in acetonitrile that demonstrated a dramatic turnaround in the initial progress toward equilibrium along the PT coordinate in the S_1 state.[31] The reversal in displacement from equilibrium that occurs in the first 300 fs is the result of ultrafast differential solvation effects between $S_1(N)$ and $S_1(T)$ following the initial excitation. In this study, we expand these results and extend the investigation to a complete series of AAQs providing new insights when ESIPT takes place as well as when it does not. For example, the negative solvatochromic shift observed in all of the AAQs has previously been considered an indication of a consistent reduction in the magnitude of the dipole moment following excitation.[26] Although the shared solvatochomic behavior does suggest a common change in the solvent−solute interaction upon excitation of all four AAQs, our direct measurements of the change in the intermolecular response demonstrate that the sign of the change is actually opposite for AAQs that favor ESIPT thermodynamically compared to those that do not. When ESIPT does take place, we not only observe changes in the intermolecular response due to changes in the solvent−solute electrostatic interactions but the exothermic reactions also create subpicosecond increases in the local solvent kinetic energy that subsequently relax by intermolecular energy exchange with the bulk solvent. The results presented here, directly monitoring the solvent response, taken in conjunction with previous investigations focusing on the solute dynamics, provide a more complete picture of the excited-state dynamics in 1-acylaminoanthraquinones.

2. Experimental Methods

2.1. Sample Preparation. HPAQ, 1-(heptanoylamino)anthraquinone, was prepared using a method analogous to that reported previously for 1-(stearolylamino)anthraquinone.[32] 1-aminoanthraquinone (3 g; Matheson, Coleman & Bell, 98% pure) was dissolved in nitrobenzene (20 mL; Avocado, 99% pure). Heptanoyl chloride (1.386 mL; Aldrich, 99% pure) was added to this, and the mixture was stirred under nitrogen for approximately 4 h. The nitrobenzene was removed by a bulb-to-bulb distillation, and the HPAQ was recrystallized from hexane. The resulting crystals were purified via column chromatography using hexanes followed by a mixture of 2:1 ethyl acetate/hexane with 3% triethylamine on silica gel.

CAAQ, 1-(chloroacetylamino)anthraquinone, was prepared on the basis of the previously reported synthesis.[33] Briefly, 1-aminoanthraquinone (2 g; Matheson, Coleman & Bell, 98% pure) was dissolved in nitrobenzene (16 mL; Avocado, 99% pure). Chloroacetyl chloride (0.713 mL; Acros Organics, 98% pure) was added to this, and the mixture was stirred under nitrogen for approximately 4 h. Excess nitrobenzene was removed by vacuum filtration and bulb-to-bulb distillation. The resulting crystals were rinsed with methanol and purified via column chromatography using a mixture of 2:1:1 chloroform/ethyl acetate/hexane with 3% triethylamine on silica gel.

DCAQ, 1-(dichloroacetylamino)anthraquinone, was prepared in an analogous manner to CAAQ. 1-aminoanthraquinone (3 g; Matheson, Coleman & Bell, 98% pure) was dissolved in nitrobenzene (24 mL; Avocado, 99% pure). Dichloroacetyl chloride (1.396 mL; Lancaster Synthesis Inc.) was added to this, and the mixture was stirred under nitrogen for approximately 4 h. Nitrobenzene was removed by vacuum filtration, and the crystals were rinsed with methanol to remove unreacted starting material. The crystals were recrystallized twice from methanol and further purified via column chromatography with 1:5 ethyl acetate/hexane with 3% triethylamine, gradually increasing the ethyl acetate component on silica gel.

TFAQ, 1-(trifluoroacetylamino)anthraquinone, was prepared as detailed previously.[34] 1-aminoanthraquinone (2 g; Matheson, Coleman & Bell, 98% pure) was dissolved in nitrobenzene (25 mL; Avocado, 99% pure). Trifluoroacetic anhydride (2.53 mL; Acros Organics, 99% pure) was added to this, and the mixture was stirred under nitrogen for approximately 1 h. Nitrobenzene was removed by vacuum filtration, and the crystals were rinsed with methanol to remove unreacted starting material. The crystals were further purified via column chromatography with 1:2 ethyl acetate/hexane with 3-triethylamine on silica gel. The TFAQ was recrystallized from methanol.

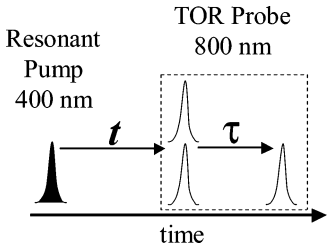

Figure 3. RaPTORS pulse sequence.

For all compounds, NMR and UV−Vis spectra were taken to ensure the purity and removal of all solvents.

2.2. Static Spectroscopy. Absorption spectra were recorded on a Jasco V-530 spectrophotometer. Fluorescence excitation and emission spectra were recorded on a Jasco FP-6200 spectrofluorimeter. The molecules were excited at 400 nm, and the spectra were corrected for the instrument response using a series of external standards: quinine sulfate, fluorescein, sulforhodamine 101, and nile blue perchlorate.[35]

2.3. RaPTORS Measurements. The experimental setup has been described previously.[29,30] The RaPTORS technique consists of an electronically resonant pump pulse followed by a third-order nonresonant Raman probe. The resonant pump pulse is centered at 400 nm and has a full width at half-maximum, fwhm, of 45 fs. Following excitation of the solute by the pump pulse, a set of three electronically nonresonant laser pulses centered at 800 nm, 40 fs fwhm, probe the third-order intermolecular Raman (TOR) response. The experiment involves two adjustable time delays, shown schematically in Figure 3. There is the delay between the resonant pump and TOR probe labeled t and a delay that is intrinsic to the TOR probe, between the coincident first two nonresonant pulses and the third nonresonant pulse, labeled τ. Samples flow through a 1 mm path length cell with 1 mm fused silica windows at a rate of roughly 0.5 mL/s. The optical density of each sample is 0.4 at 400 nm, indicating sample concentrations of $\sim 1 \times 10^{-3}$ M. Time resolution along the t dimension is limited by the group velocity mismatch between the 400 and 800 nm laser pulses, resulting in an instrument response function with a 150 and 170 fs fwhm (Gaussian) for CH_3CN and CH_2Cl_2, respectively. Time resolution in the τ time dimension is determined by the cross-correlation of the 800-nm laser pulses. Acetonitrile (Pharmco, HPLC grade) and dichloromethane (Fisher, ACS grade) are used as received. All of the measurements are performed at room temperature.

The RaPTORS technique provides a measurement of the change in the intermolecular Raman response because of resonant solute excitation. The 400 nm pump pulse is modulated at half of the laser repetition rate, and the signal, measured by lockin detection at the modulation frequency, reflects the *change* in the TOR response following resonant excitation, $\Delta E^{(3)}(t, \tau)$. The measured signal is a cross term between $\Delta E^{(3)}(t, \tau)$ and the nonresonant TOR signal field from the bulk solvent that is present with and without the pump pulse, $E^{(3)}_{\text{solvent}}(\tau)$.[29,30]

$$I_{\text{RaPTORS}}(t, \tau) \propto \Delta E^{(3)}(t, \tau)\, E^{(3)}_{\text{solvent}}(\tau) \qquad (1)$$

The electronically nonresonant TOR probe interrogates the intermolecular nuclear response via the third-order time domain response function, which can be expressed in terms of a polarizability correlation function[36]

$$E^{(3)}(\tau) \propto R^{(3)}(\tau) = -\frac{i}{\hbar}\langle[\alpha(\tau),\alpha(0)]\rangle \qquad (2)$$

The proportionality becomes equal in the impulsive limit.

In the work reported here, the value of τ is held fixed and the t delay is scanned. These scans are referred to as t-slices. Setting a fixed value of τ and collecting the response along t has two important consequences. First, the value of $E^{(3)}_{\text{solvent}}(\tau)$ in eq 1 is a constant for fixed τ and thus acts as a time-*in*dependent local oscillator. Second, the value of the fixed τ delay dictates the point in the nuclear polarizability response that is probed as a function of t. In this study, we focus our discussion on t-slices near the peak of the intermolecular polarizability response at $\tau = 140$ fs in acetonitrile and $\tau = 180$ fs in dichloromethane. This portion of of the response is often associated with libration motions, but these fastest solvent time scales are likely to include translational motions as well.[37−41] We have chosen to probe near the peak of the intermolecular response in this initial study because this point in the response is sensitive to changes in the intermolecular solvent−solute interactions and changes in the kinetic energy of the solvent.[30] The heterodyne-detected nonresonant TOR responses for acetonitrile and dichloromethane are shown in the Supporting Information, with the fixed value of τ used in the t slices indicated for reference. Recovery of the change in the complete intermolecular response as a function of the t delay is complicated significantly by the time dependence of the intrinsic local oscillator along τ,[30] and this will be addressed in a forthcoming manuscript.[42] The response at a larger value of τ is discussed briefly in section 4.5. Raw data, fits, and fitting parameters for t-slices at $\tau = 350$ fs in acetonitrile and $\tau = 360$ fs in dichloromethane are available in the Supporting Information.

To suppress the instantaneous electronic response in the TOR probe, we set the three linearly polarized nonresonant laser fields and the detected signal to select the following tensorial portion of the response:[43,44]

$$3R^{(3)}_{yyxx}(\tau) - R^{(3)}_{xxxx}(\tau) = R^{(3)}_{dcxx}(\tau) \qquad (3)$$

The relative laser polarization angles are indicated with respect to x, where $d = -71°$, $c = 45°$, and $y = 90°$. Selection of this tensorial response results in negative signal amplitudes for intermolecular motions (for example, see the heterodyne-detected TOR solvent measurements provided in the Supporting Information).[44] A negative TOR response not only means that increases in the intermolecular polarizability response are indicated by a decrease (more negative) in the signal, that is, $\Delta E^{(3)}(t; \tau) < 0$, but it also means that the local oscillator is negative, $E^{(3)}_{\text{solvent}}(\tau) < 0$. The measured signal intensity is the product of these two contributions, see eq 1, and thus increases in the TOR response caused by the action of the resonant excitation pulse result in positive RaPTORS signals, whereas decreases result in negative RaPTORS signals.[30]

2.4. Computational Methods. The optimized structures, used as starting points for all of the energetic and dipole calculations, were determined using Gaussian 98.[45] The DFT method used for the optimizations was Becke's three-parameter hybrid functional using the correlation functional of Lee, Yang, and Parr, B3LYP.[46−48] The MIDI! basis set was used for all of the DFT calculations.[49] The MIDI! basis set has been shown to provide more accurate geometries and charge distributions than the 6-31G* basis set at significantly reduced computational cost for medium and large size molecules.[49] The OH bond distance in the proton-transfer tautomer was constrained to 0.97−1.01 Å to prevent back transfer during the optimization of the ground electronic state. In the normal species, frequency calculations were carried out to verify stationary points. Gas-phase polar-

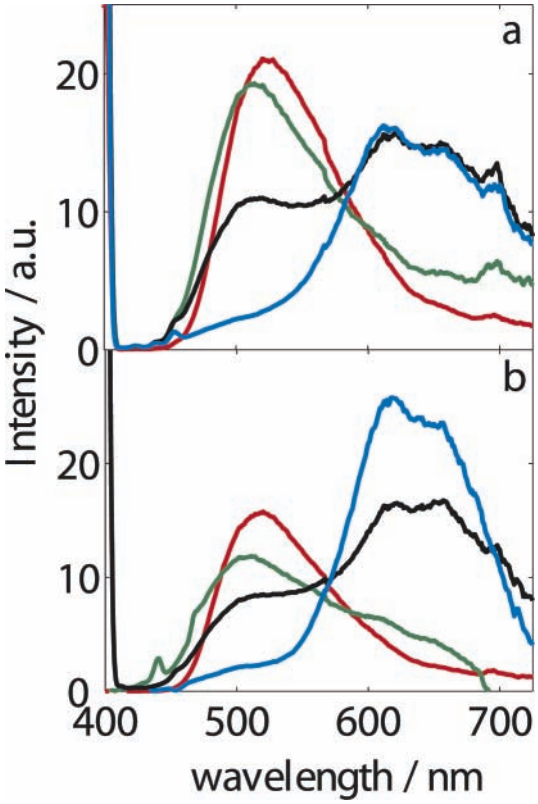

Figure 4. Static fluorescence spectra for AAQs in acetonitrile (a) and dichloromethane (b). All species were excited at 400 nm, and the spectra were corrected for the instrument response. Red, HPAQ; green, CAAQ; black, DCAQ; blue, TFAQ.

izabilities were calculated from the optimized B3LYP/MIDI! structures. The excitation energies and dipole moments of the AAQs in acetonitrile and dichloromethane are SM5.42/INDO/S2 values calculated by the ZINDO-MN program.[50] ZINDO-MN incorporates the INDO/S2 parameters, the CM2 charge model, the SM5.42R continuum solvation model, and the VEM42 vertical excitation model for nonequilibrium electrostatic free energies of solvation.[51,52] The CIS active space for VEM42 calculations was (10, 10), allowing substitutions from the 10 highest HOMOs (highest occupied molecular orbitals) to the 10 lowest LUMOs (lowest unoccupied molecular orbitals). The ZINDO-MN program was selected for its abililty to provide accurate excited-state CM2 dipole moments and excitation energies, which include solvent effects within the SM5.42 continuum model, at reasonable computational cost. Solvent descriptors for acetonitrile and dichloromethane were taken from the Minnesota Solvent Descriptor Database.[53]

3. Results and Analysis

3.1. Static Spectroscopy. The absorption spectra for all four AAQs in both acetonitrile and dichloromethane are available in the Supporting Information. The static fluorescence spectra for the AAQs in acetonitrile and dichloromethane are shown in Figure 4. All species were excited near the peak of the absorbance at 400 nm. Emission from the normal species is centered near 510 nm, and the proton-transfer species is characterized by emission around 635 nm.[25] The absorption and fluorescence spectra are consistent with the previous report of Smith et al.[25] As illustrated in Figure 4, the fluorescence from HPAQ is dominated by the shorter wavelength component assigned to the normal form, whereas the emission from TFAQ is dominated by the longer wavelength emission of the tautomer. DCAQ and CAAQ exhibit dual emission in both solvents with an increase in the intensity from the tautomeric versus normal form in dichloromethane compared to acetonitrile. The ratio of $S_1(T)$ to $S_1(N)$ emission is larger for DCAQ than CAAQ in both solvents.

3.2. RaPTORS *t*-Slices. RaPTORS *t*-slices were each fit as the sum of the following three components: a dynamic change in the intermolecular solvent response following solute excitation, a decay due to loss of anisotropy in the initially prepared system that follows solute rotation, and the neat solvent background. A description of each of these signal contributions follows.

The TOR probe of the intermolecular response can both increase and decrease with time, depending on the dynamic changes of the system that follow electronic excitation of the AAQ chromophore. The origins of both positive and negative changes in the signal will be discussed in section 4. The excited-state lifetimes of the AAQs are comparable to, or, in some cases, much longer than the experimental capabilities of our delay stages. As a result, changes in the intermolecular response may persist well beyond our longest experimental delay time.[30] To allow for multiple positive and negative time-dependent changes, we have chosen to model the observed signal as a series of events, eq 4.

$$a(t)\mathbf{A} \xrightarrow{t_1} b(t)\mathbf{B} \xrightarrow{t_2} c(t)\mathbf{C} \xrightarrow{t_3} d(t)\mathbf{D} \xrightarrow{t_4} e(t)\mathbf{E} \qquad (4)$$

In eq 4, capital letters **A**−**E** represent the values of the change in the TOR probe at different points in time. The time-dependent weighting factors, $a(t)-e(t)$, can each have values in the range 0−1, and are constrained to sum to 1 at all times. The initial conditions are defined by $a(t = 0) = 1$, and t_1-t_4 are the time constants for transitions between the different signal values. An analytical form for the time-dependent values of the weighting factors in terms of the time constants was obtained by solving the associated set of differential equations, and this is outlined in the Supporting Information. The contribution to the time-dependent signal, eq 1, is then simply the weighted sum of the values in the series

$$I(t;\tau) = a(t)\mathbf{A} + b(t)\mathbf{B} + c(t)\mathbf{C} + d(t)\mathbf{D} + e(t)\mathbf{E} \qquad (5)$$

Values **A**−**E** and time constants t_1-t_4 are treated as variable parameters when fitting the data, and the result is convoluted with the instrument response function prior to comparison with the data during optimization. Optimizations of the fits to the data are started with the four steps shown in eq 4. If the values of two or more time constants converge during the optimization, indicating an inability to resolve individual events, then the redundant steps are removed from the response.

Because of the anisotropic portion of the nonresonant TOR probe and the anisotropic distribution of chromophores excited by the linearly polarized pump pulse, there is a decay component in the measured signal that reflects solute rotation. The solute rotational component is modeled as an exponential decay, $R_{\text{rotation}}(t) = Ae^{-t/\tau_{\text{rot}}}$, where the amplitude, A, and rotation time constant, τ_{rot}, are variable parameters in the fitting. The rotational decay is convoluted with the instrument response function prior to comparison with the raw data in the optimization procedure. The rotation times determined for the AAQs, reported in Tables 1 and 2, are in qualitative agreement with rotation times determined for a dye molecule of similar size, Coumarin 153, in these solvents.[54]

The solvent background is determined from the neat solvent measured under the identical conditions as the RaPTORS data. In the absence of chromophore, there is a signal centered at

TABLE 1: Fitting Parameters for RaPTORS *t*-slices for AAQs in Acetonitrile[a]

	A	*B*	*C*	*D*	*E*	t_1 (ps)	t_2 (ps)	t_3 (ps)	t_4 (ps)	τ_{rot} (ps)
HPAQ	0.0	−24.0	−4.7			0.39	450			23
CAAQ	−7.3	17.0	4.5	−10.0	−1.4	0.10	0.18	1.1	160	16
DCAQ	0.0	34.3	34.4	15.1	−1.7	0.20	1.1	12.2	106	21
TFAQ	0.0	48.0	34.9	17.3	−1.9	0.27	3.4	9.8	94	21

[a] See section 3.2 of the text for a description of the listed values.

TABLE 2: Fitting Parameters for RaPTORS *t*-slices for AAQs in Dichloromethane[a]

	A	*B*	*C*	*D*	*E*	t_1 (ps)	t_2 (ps)	t_3 (ps)	t_4 (ps)	τ_{rot} (ps)
HPAQ	0.0	−15.3	−18.0	−1.3		0.61	3.6	705		30
CAAQ	−3.1	16.0	3.0	−2.1	−2.5	0.13	1.7	12.5	96	24
DCAQ	0.0	40.0	33.1	13.0	−0.4	0.22	1.2	15.5	105	28
TFAQ	0.0	39.1	32.4	12.3	−0.2	0.18	3.5	11.5	110	27

[a] See section 3.2 of the text for a description of the listed values.

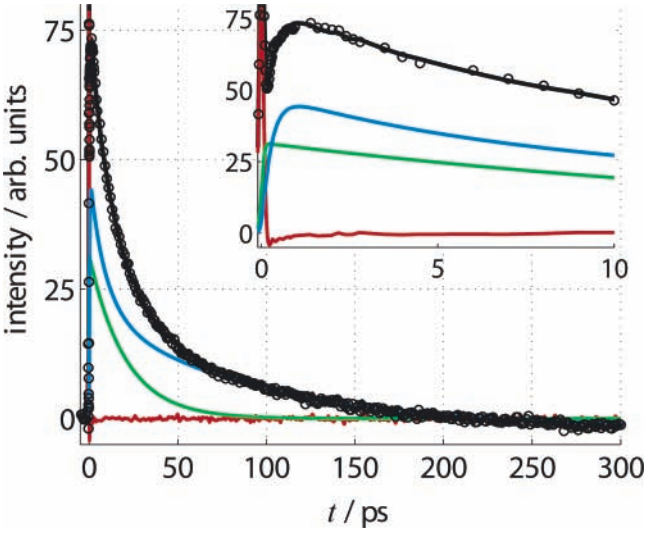

Figure 5. RaPTORS *t*-slice for TFAQ in acetonitrile at $\tau = 140$ fs showing the raw data (points), complete fit, and individual fit components. Details of the fitting are described in section 3.2. Black, total fit; red, neat solvent background; green, solute rotation; blue, dynamic solvent response.

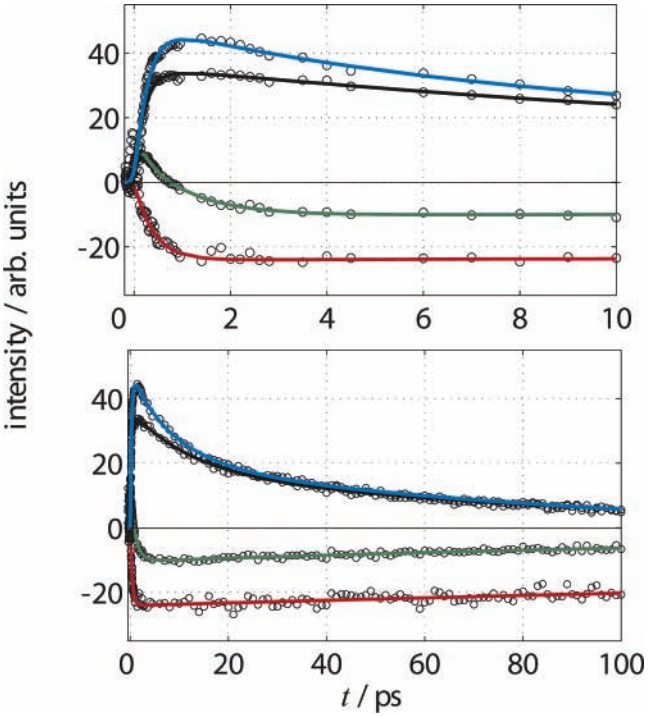

Figure 6. RaPTORS *t*-slices for all AAQs in acetonitrile at $\tau = 140$ fs showing the data (points) and fit as described by eq 4. Red, HPAQ; green, CAAQ; black, DCAQ; blue, TFAQ.

$t = 0$ fs that results from electronically nonresonant interactions of the 400 and 800 nm laser pulses. The intensity of this background feature is reduced in solutions that contain the AAQs because of resonant absorption of the 400 nm pulse. Comparison of the peak intensity at $t = 0$ fs demonstrates a reduction in the signal intensity consistent with the optical density of the sample, indicating that in the AAQ samples the time resolution limited feature at $t = 0$ fs is dominated by the neat solvent background. After linear scaling of the neat solvent response to account for the change in the optical density at 400 nm, the signals from the neat solvent are included directly as fixed components in the fit to the data.

The raw data and complete fit are shown in Figure 5 for the *t*-slice at $\tau = 140$ fs for TFAQ in acetonitrile. The raw data and complete fits for all AAQs in both acetonitrile and dichloromethane are available in the Supporting Information. To emphasize the dynamic events of interest, we present the raw data and fits following subtraction of the neat solvent background and exponential decay due to molecular rotation in Figures 6 and 7. The fitting parameters are listed in Tables 1 and 2 for acetonitrile and dichloromethane. All of the compounds show a long time (>90 ps) decay of the signal intensity associated with the lifetime of the excited states. Early time dynamics vary by AAQ, and they are discussed in detail in section 4. DCAQ and TFAQ exhibit an initial 100−200 fs rise followed by a 1−2 ps event, and these time scales shift slightly longer in dichloromethane. For CAAQ in acetonitrile, the solvent response contains two subpicosecond time scales, a 100 fs increase followed by 180 fs and 1.1 ps decreases.[31] In HPAQ, there is a single negative component with a time constant of 425 fs in acetonitrile and 610 fs in dichloromethane. In the AAQs where tautomeric emission is significant, there is an additional decay component of ca. 10 ps. This time scale is present for DCAQ and TFAQ in both solvents and CAAQ in dichloromethane.

3.3. Computational Results. Tables 3 and 4 summarize the computational results for the AAQs in terms of bond distances, bond angles, molecular dipole moments, and excitation energies. The reported bond lengths and angles at the site of intramolecular PT are shown in Figure 1. The bond lengths are indicative of strong intramolecular hydrogen bonds for all AAQs in both the normal and tautomeric species with an average hydrogen bond length of 1.7 and 1.6 Å in the normal and tautomeric forms, respectively. The angle of the hydrogen bond, with the vertex at the transferring proton is 140° in the normal species and 150° in the tautomeric species.

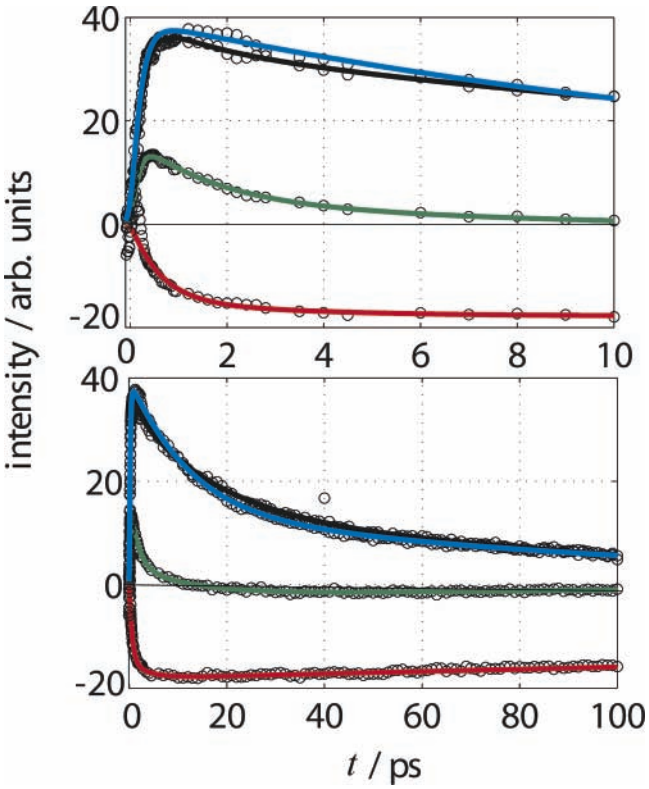

Figure 7. RaPTORS *t*-slices for all AAQs in dichloromethane at $\tau =$ 180 fs showing the data (points) and fit as described by eq 4. Red, HPAQ; green, CAAQ; black, DCAQ; blue, TFAQ.

TABLE 3: B3LYP/MIDI! Optimized Ground State AAQ Structural Parameters[a]

		r_{O-H} (Å)	r_{N-H} (Å)	θ_{N-O-H} (deg)
HPAQ	N	1.72	1.04	141.6
	T	0.98	1.56	152.8
CAAQ	N	1.73	1.04	138.7
	T	0.98	1.58	149.6
DCAQ	N	1.70	1.05	140.8
	T	0.99	1.57	150.8
TFAQ	N	1.71	1.04	140.0
	T	0.99	1.56	150.6

[a] Structures Are Shown in Figure 1

The dipole moments increase upon vertical excitation of S_0(N) for HPAQ and CAAQ, and decrease for DCAQ and TFAQ in both solvents. The dipole moments of all AAQs decrease upon vertical excitation of S_0(T). In the excited state, with the exception of TFAQ, the dipole moment is reduced upon going from the S_1(N) to S_1(T) (i.e., upon ESIPT). In all of the AAQs studied, the dipole moment is similar in direction for S_0(N) and S_1(T). There is a significant directional change that accompanies the change in magnitude between S_0(N) and S_1(N). This is shown in Table 4, where the angle was determined by overlapping the structures and comparing the angle between the dipole moments of S_1(N) and S_1(T) with S_0(N) for the given AAQ. When comparing the dipole directions between the normal and tautomeric structures, the molecules were aligned to provide the best possible overlap of the atomic positions for the oxygen, nitrogen, and three intervening carbons at the proton-transfer sites.

The calculated and experimental excitation energies are presented in Table 4. The VEM42/ SM5.24/INDO/S2 vertical excitation model agrees well with the experimental excitation energy of the normal species. There is a shift to higher excitation energies for the species as the acyl group becomes more electrophilic, from HPAQ to TFAQ, as seen in the experimental absorption spectra. Excitation of the tautomer is shifted about 4000 cm^{-1} compared to the normal species, largely because of the relative instability of the tautomeric ground state. The excitation energies for the proton-transfer tautomers show the same increase in excitation energy with acyl group electrophilicity as in the normal species. Inclusion of the SM5.42 solvation model results in a blue shift of the excitation energies for all AAQs when increasing the polarity of the solvent from dichloromethane to acetonitrile, in agreement with experiment. Given the increase in magnitude of the dipole moment upon excitation in only two of the four AAQs, the negative solvatochromic shift that is common to all of the AAQs is due primarily to the large change in the angle of the dipole moment that accompanies transition to the S_1 state. Negative solvatochromic shifts due to changes in the dipole angle have been demonstrated experimentally for several dye molecules.[55]

The RaPTORS experiments are sensitive to changes in the AAQ−solvent interactions after resonant excitation.[30] Changes in the electrostatic portion of the solvent−solute interaction that accompany both excitation and ESIPT are approximated with the solvent polarization energy of the Kirkwood−Onsager continuum dielectric model.[56−58]

$$G_p = -\frac{1}{2}\left[\frac{2(\epsilon - 1)}{(2\epsilon + 1)}\right]\frac{\mu^2}{a^3} \qquad (6)$$

In eq 6, a is the radius of solute, assumed to be spherical, and is fixed at 4.4 Å on the basis of the calculated molecular volumes. The dielectric constant at 298 K for acetonitrile is $\epsilon = 35.69$,[53] for dichloromethane it is $\epsilon = 8.93$,[53] and the dipole moments, μ, are taken from Table 4. The resulting solvent polarization energies are presented in Table 5. We acknowledge the quantitative shortcomings of eq 6, including the fact that the AAQs are clearly not spherical and the approximation of the multipole expansion with only the dipolar term.[56] However, we believe it is reasonable as an indication of the sign and relative magnitude of the changes in the solvent−solute interaction when comparing different structures and states of the AAQs. Changes in the electrostatic interactions that result from excitation, $S_0 \rightarrow S_1$, differ depending on the acyl substituent as a result of the different sign of the changes in the magnitude of μ, see Table 4. The excited states are stabilized relative to the ground states for HPAQ and CAAQ, whereas the electrostatic interaction decreases in DCAQ and TFAQ.

In addition to the electrostatic contributions to the solvent−solute interaction, there will also be dispersion, and there could be specific interactions such as hydrogen bonding. For the solvents in this study, acetonitrile and dichloromethane, we assume that any hydrogen bonding interactions are small compared to the electrostatic and dispersion interactions. Our ability to assess contributions from the dispersion interactions in these condensed phase systems is limited. With small differences in the solute's molecular polarizabilty between the normal and tautomeric forms, we assume that the change in the dispersion interaction with PT is small. In the case of the electronic transition, $S_0(N) \rightarrow S_1(N)$, the dispersion interaction is expected to increase (lower the solvation energy) as indicated by modest increases in the AAQ's molecular polarizability. Using finite field calculations at the HF/MIDI! and CIS/MIDI! level, we calculate a ca. 10% increase in the polarizability from S_0(N) to S_1(N) in both HPAQ and TFAQ. On the basis of this, we predict a small, consistent increase in the dispersion interaction for all of the AAQs studied. We emphasize that we

TABLE 4: ZINDO-MN Dipole Moments and Vertical Transition Energies

		dipole moment[a]						vertical excitation energy[b]	
		CH_3CN			CH_2Cl_2				
		S_0	S_1	angle	S_0	S_1	angle	CH_3CN	CH_2Cl_2
HPAQ	N	5.7	6.9	39	5.5	6.7	40	25 647(24 631)	25 564(24 272)
	T	8.5	5.2	17	8.3	4.8	18	21 822	21 742
CAAQ	N	4.1	5.1	56	3.9	5.0	53	25 895(25 575)	25 819(25 381)
	T	7.7	3.4	12	7.9	3.0	8	21 952	21 848
DCAQ	N	4.5	4.4	54	4.4	4.3	56	25 980(25 907)	25 899(25 641)
	T	8.5	3.9	11	8.4	3.6	13	21 947	21 832
TFAQ	N	5.6	4.3	44	5.6	4.2	45	26 024(26 525)	25 939(26 178)
	T	10.6	5.7	14	10.2	5.3	17	22 085	21 961

[a] The dipole moments are in Debye. The angles are in degrees and indicate the angle between the S_1 dipole moment and the S_0(N) dipole moment. [b] Vertical excitation energies are reported in cm^{-1}. Experimental absorption maxima are given in parentheses for comparison.

TABLE 5: Solvent Polarization Energies, G_P[a]

		HPAQ		CAAQ		DCAQ		TFAQ	
solvent	structure	S_0	S_1	S_0	S_1	S_0	S_1	S_0	S_1
CH_3CN	N	−919	−1347	−476	−736	−573	−548	−887	−523
	T	−2044	−765	−1677	−327	−2044	−430	−3179	−919
CH_2Cl_2	N	−751	−1114	−378	−621	−481	−459	−778	−438
	T	−1710	−572	−1549	−223	−1751	−322	−2582	−697

[a] All values reported in cm^{-1}. See section 3.3 and eq 6 for details.

are not suggesting that the dominant contribution to the solvation energy for a given state of an AAQ is electrostatic, only that *changes* in the solvent−solute interaction associated with excitation and PT will have the largest influence from the electrostatic changes. This is a better assumption in acetonitrile than dichloromethane because of the larger molecular polarizability of dichloromethane. The results discussed in section 4 are consistent with the changes predicted by the electrostatic interactions in both solvents.

4. Discussion

First, we consider some general observations from the complete set of AAQs investigated, and this is followed by more specific discussions of the individual AAQ dynamics. In Figures 6 and 7, the series of AAQs clearly present contrasting RaPTORS responses, with a negative response for HPAQ, and increasingly positive responses for CAAQ, DCAQ, and TFAQ. In Figures 6 and 7, near the peak of the nonresonant TOR solvent response, changes in this response are sensitive to changes in the intermolecular solvent−solute interactions and changes in the solvent kinetic energy.[30] Increases in the solvent−solute interaction (more negative interaction energy) decrease the TOR response, and decreases in the interaction increase the TOR response. Changes in the solvent kinetic energy produce the opposite trend, with increasing kinetic energy resulting in an increase in the TOR response.

The trends in the RaPTORS responses are consistent with the changes in solvent−solute interactions predicted in section 3.3 and shown in Table 5. For HPAQ, where ESIPT is restricted, the change reflects the difference between excited and ground state of the normal form, S_1(N) and S_0(N), where the intermolecular interaction increases. When ESIPT takes place, the signal reflects contributions from both S_1(N) and S_1(T), with the relative weight of the contributions depending on the extent of PT. In the cases that favor ESIPT, TFAQ and DCAQ, there is a decrease in the solute−solvent interaction comparing the excited-state species with S_0(N). In addition to the reduction in solvent−solute interactions, the initial positive responses from TFAQ and DCAQ also reflect some heating of the solvent that follows from the exothermic PT, and this will be discussed in section 4.2. Table 5 shows that in CAAQ, relative to S_0(N), there is an increase in the intermolecular interaction for S_1(N) and a decrease for S_1(T). The responses show complex behavior at early times with an instantaneous decrease followed by both an increase and subsequent decrease within the first picosecond after excitation. These dynamics in CAAQ reflect rapid changes in the S_1(N)/S_1(T) ratio after excitation and are discussed in section 4.3.

Comparison of the *t*-slices in acetonitrile and dichloromethane, Figures 6 and 7, are consistent with the changes in the ratio of static fluorescence from S_1(N) and S_1(T).[25] In the limiting ESIPT cases there are very little changes, with HPAQ dominated by S_1(N) and TFAQ dominated by S_1(T) in both solvents. Only subtle changes in the *t*-slices are observed in these AAQs. Both DCAQ and CAAQ have a clear increase in the S_1(T)/S_1(N) fluorescence ratio in dichloromethane, and in both cases the RaPTORS response shows an associated increase. The DCAQ response increases to become very similar to the TFAQ response in dichloromethane, and the majority of the CAAQ response changes sign from negative to positive when going from acetonitrile to dichloromethane.

The solvent-dependent changes in the static fluorescence,[25] pump−probe,[27] and the RaPTORS responses reported here for CAAQ all indicate that increases in solvent polarity stabilize S_1(N) relative to S_1(T). From the negative solvatochromic shift and a semiemperical calculation on an AAQ model compound, 1-hydroxyanthraquinone, Smith et al. concluded that there is a reduction in the dipole moment upon excitation of the AAQs, $S_0(N) \rightarrow S_1(N)$.[25] The negative RaPTORS response for HPAQ and CAAQ are not consistent with this conclusion and provide direct evidence of an increase in the solvent−solute interaction from the ground to excited state of the normal form. Our calculations indicate that in these two AAQs, where S_1(N) is the more intense fluorescence species, there is an increase in the solvent−solute interaction that comes from an increase in the magnitude of the dipole moment. The negative solvatochromic shift in these compounds must be the result of the large change in the angle of the dipole moment upon excitation, ca.

45 ° as shown in Table 4. For compounds that strongly favor PT in the excited state, such as TFAQ and the model compound 1-hydroxyanthraquinone, our results agree with the conclusion that there is a reduction in the dipole moment with excitation of the normal form. In the case of TFAQ, the negative solvatochromic behavior originates from a combination of a decrease in the magnitude and significant change in the direction of the dipole moment between $S_1(N)$ and $S_0(N)$. Together, these results highlight the differences in how solvent−solute interactions change after excitation depending on the acyl substituent, with similar changes among the endothermic ESIPT variants, HPAQ and CAAQ, and among the exothermic ESIPT variants, DCAQ and TFAQ. This also indicates that using any single model system to interpret the excited-state dynamics in solution across this entire series of AAQs is not sufficient.

4.1. HPAQ: Restricted ESIPT. In both acetonitrile and dichloromethane, the static fluorescence spectrum of HPAQ indicates the presence of very little, if any, excited-state tautomeric form. Time-resolved fluorescence demonstrates that if there is ESIPT within this system then it is either followed by nearly instantaneous back transfer or it is a very slow ($\gg$100 ps) process.[25] The RaPTORS *t*-slices indicate two main time scales for HPAQ, a fast initial decay followed by a long time scale increase toward zero. The initial decrease in the response is due to the sudden increase in the solvent−solute interactions following excitation, and subsequent solvent reorganization (solvation) in the $S_1(N)$ state serves to further lower the intermolecular interaction energy. This occurs with a time constant of 425 fs in acetonitrile, midway between the inertial, 89 fs, and diffusive, 630 fs, time scales for dipolar solvation in acetonitrile.[59] In dichloromethane, the time constant for the initial decay of the RaPTORS *t*-slice is 610 fs, lying between the experimentally determined inertial, 144 fs, and diffusive, 1.02 ps, time scales for dipolar solvation.[59] The increase in the time scale with solvent is consistent with the increased solvation times in dichloromethane.

Following solvation, there is a long time decay in the magnitude of the signal that measures the declining difference in the solvent−solute interaction as the population of the excited-state $S_1(N)$ decays. The time constants of this decay, in both solvents, exceeds the length of the scanning delay stage. By fixing the final time constants to the reported fluorescence lifetimes of 450 and 705 ps observed in acetonitrile and dichloromethane,[25] excellent agreement is found with our measured responses. However, even with the inclusion of this very long decay due to the excited-state lifetime, the final value in the fitting, see Tables 1 and 2, does not return to zero. The fact that a difference in the solvent response remains indicates that relaxation from the excited state is not exclusively to the original ground state. We attribute this to some degree of intersystem crossing (ISC) to the triplet state, as illustrated in Figure 2. ISC has been determined to be a competitive excited-state process in AAQs, with microsecond lifetimes reported for the triplet state.[28] The negative final value in the RaPTORS fit indicates a larger solvent−solute interaction for $T_1(N)$ than $S_0(N)$, due most likely to a larger dipole moment in the triplet state.

4.2. TFAQ and DCAQ: Rapid ESIPT. The static emission from TFAQ is dominated by the tautomeric species, and this is the larger component for DCAQ in both solvent environments. Smith et al. measured an instrument-limited ($<$350 fs) appearance of $S_1(T)$ for both TFAQ and DCAQ. The *t*-slices in Figures 6 and 7 show that in both solvents the initial response is a rapid increase with a time constant of ca. 200 fs. The response then turns over and declines on two time scales, ca. 10 ps and ca. 100 ps. The largest time constants are in good agreement with excited-state lifetimes measured by fluorescence of 99 and 125 ps for DCAQ, and 116 and 119 ps for TFAQ in acetonitrile and dichloromethane.[25] The rapid 200 fs rise is likely to come from a combination of a reduction in the solvent−solute interaction and an increase in the kinetic energy of the solvent. Table 5 shows that following excitation there is a decrease in the intermolecular interaction. After ESIPT, the solvent polarization returns to a value similar to $S_0(N)$. As mentioned previously, one of the assumptions in Table 5 was that the same cavity radius describes both the ground and excited states. A small increase in the molecular size on going from the ground to excited state would produce an additional net increase in the solvent polarization energy. The result would be a reduction of AAQ-solvent interactions in both $S_1(N)$ and $S_1(T)$ relative to $S_0(N)$, in agreement with our measurements. However, the subsequent ca. 10 ps decrease in the signal, recovering to about half of the initial increase, is not consistent with only this one origin for the initial increase. Changes in the intermolecular interaction are established within the first picosecond and should persist for the lifetime of the newly created state as seen in HPAQ.

The ca. 10 ps decline in the *t*-slices is exhibited only in AAQs in which PT in the excited state is exothermic. We believe the solvent response when rapid ESIPT takes place has an additional contribution from the energy released during chemical reaction. This results in an initial kinetic energy gain in the local solvent environment. An estimate from the ratio of the normal and tautomer emission intensities indicates that ESIPT is exothermic by roughly 2 kcal/mol at room temperature.[25] During ESIPT, energy is transferred to the local solvent environment and then subsequently dissipates into the bulk solvent. The initial increase in kinetic energy is localized in the adjacent solvent, resulting in a relatively large increase in the kinetic energy of these solvent molecules. This is reflected in a rapid increase in the RaPTORS response. As the energy is transferred into the bulk solvent, the initially excited local solvent cools and the RaPTORS response decreases. The net effect of this intermolecular energy transfer process is a rapid heating of the local solvent during the first 200 fs followed by dissipation of that energy into the bulk on an overall time scale of about 10 ps. A similar type of energy transfer has been reported in simulations that followed the initial gain and subsequent transfer of excess energy following excitation of a dye molecule in acetonitrile.[60] These simulations indicated an initial 200 fs transfer of the kinetic energy into the first solvation shell, followed by a roughly 1 ps time constant for energy flow from the first solvation shell to the second. The simulations were not over long enough time scales to reach an equilibrated energy distribution. Based on our measurements, the dissipation of the energy into the bulk is a slightly slower process in dichloromethane. These dynamics, energy transfer to and in the surrounding molecular solvent, are fundamental components of reactions in solution that are not captured in experiments designed to interrogate the solute.

The *t*-slice signal does not return to zero on the time scale of the experiment, settling to a slightly negative value at 300 ps. As in the case of HPAQ, we believe this is due to some competition in the relaxation of the S_1 state via ISC to a relatively long-lived triplet state. When ISC occurs in the tautomeric form, Nagaoka et al. have reported rapid back proton transfer from the tautomeric triplet state to the normal triplet state.[28] The negative offset indicates that the long-lived triplet

has a larger solvent−solute interaction than $S_0(N)$, which is likely due to a larger dipole moment. The triplet states are illustrated in the scheme in Figure 2.

4.3. CAAQ: An Intermediate Case. A brief initial account of results for CAAQ in acetonitrile has appeared previously in ref 31. CAAQ represents an intermediate case in which the small energetic difference between $S_1(N)$ and $S_1(T)$ amplifies the role played by solvation dynamics during ESIPT. Although ESIPT takes place rapidly in both solvents, the static fluorescence remains dominated by emission from $S_1(N)$, with an increase in the $S_1(T)/S_1(N)$ emission ratio going from acetonitrile to dichloromethane.[25,27]

The CAAQ RaPTORS *t*-slices exhibit dynamics that are not seen in either of the limiting PT cases. In both solvents, our fits start at a negative value (the value of *A* in Tables 1 and 2) indicating a reduction in the response within our time resolution, and this is followed by a 100 fs rise. Looking at Table 4, excitation of CAAQ creates an initial increase in the dipole moment in $S_1(N)$, and PT to $S_1(T)$ results in a reduction of the dipole moment relative to the initial state, $S_0(N)$. The *t*-slices follow the sudden increase in intermolecular interaction after excitation and subsequent reduction in this interaction with rapid PT. This result is in excellent agreement with the pump−probe results of Neuwahl et al., where the authors demonstrated evidence for the impulsively excited $S_1(N)$ and a delayed, 100−110 fs arrival of $S_1(T)$.[27] These authors attributed the initial dynamics to equilibration on the excited PES dictated by a barrier along the PT coordinate.

Following the initial 100 fs rise, the RaPTORS responses turn around, with a dramatic 180 fs decline in acetonitrile and 1−2-ps decreases in both solvents. On the basis of the change in intermolecular interactions, increases in the response indicate progress toward $S_1(T)$, and decreases indicate progress toward $S_1(N)$. The signal reversal in the first picosecond indicates a dynamic shift in the displacement from equilibrium along the PT coordinate in the excited state. This cannot be explained by equilibration along a time-independent PT coordinate. These results demonstrate that dynamic solvent reorganization is changing the potential energy landscape on these time scales and controlling the PT dynamics. This turnaround in the reaction is not seen in the pump−probe experiments, in which the authors chose to focus on the initial appearance of $S_1(T)$.[27] However, Smith et al. did note an interesting rise in the fluorescence from $S_1(N)$ with an exponential time constant of 850 ± 350 fs.[25] Within the quality of the data, this rise was suggested to correlate with a decrease in the emission from $S_1(T)$ that was fit to a time constant of 3 ± 1 ps. The authors tentatively assigned this behavior to differential solvation of the two excited-state species. The time constants associated with the return to $S_1(N)$ in our data confirm this general picture; however, we find differences in the underlying details. Smith et al. explained the greater solvent response in $S_1(N)$ compared to $S_1(T)$ as originating from a significant reduction in the dipole moment in $S_1(N)$, contrasting this with very similar dipole moments in $S_1(T)$ and $S_0(N)$. Our results demonstrate that there is an increase in the dipole moment for $S_1(N)$ and a decrease for $S_1(T)$, and that this is the basis for differential solvent reorganization for the two excited-state species. A simple model that includes solvent reorganization is used in the next section to illustrate this picture of coupled solvent and PT dynamics. The turnaround in the displacement from equilibrium that is driven by solvation is more subtle in dichloromethane because of smaller electrostatic solvent−solute interactions that serve to lessen the difference in stabilization of two excited-state species. In addition, the slower time constant associated with the solvent-driven energy lowering of $S_1(N)$ relative to $S_1(T)$ slows from 1.1 to 1.7 ps in accordance with observed slowing in the solvation response.[59]

Beyond the initial dynamics, there is a general positive offset of the *t*-slice in dichloromethane compared with acetonitrile, in agreement with the larger $S_1(T)/S_1(N)$ ratio found in the static emission. The longest time constants, 160 ps in acetonitrile and 96 ps in dichloromethane, agree with the associated measured fluorescence lifetimes of 151 and 107 ps, respectively.[25] As in the case of the other AAQs, the RaPTORS responses do not return to zero on the time scales determined in the experiment. The negative asymptotic values in both solvents (the value of E in Tables 1 and 2) are assigned to competing ISC pathways that result in long-lived triplet states[28] with larger dipole moments than $S_0(N)$.

4.4. A Simple Model. The CAAQ dynamics indicate that solvent reorganization cannot be separated from the proton-transfer dynamic. Differential solvation of the excited-state normal and tautomeric species competes with the PT time scales within the first picosecond after excitation, creating a strong correlation between the solvent and PT dynamics. Beyond the inertial response, time scales >1 ps, motion along the PT coordinate becomes rapid compared with solvent reorganization. This leaves the dynamics controlled by diffusive solvation on these longer time scales, driving evolution of the equilibrium position along the PT coordinate.[61] Here we consider a simple model to illustrate the effect of combined PT and solvent coordinates for the cases of CAAQ and TFAQ in acetonitrile. This will show that displacement along a solvent coordinate can produce a dramatic change in the relative energies of $S_1(N)$ and $S_1(T)$. It will also demonstrate the effect of displacement of $S_1(N)$ and $S_1(T)$ in the excited state relative to the solvent configuration at $t = 0$ determined by $S_0(N)$.

The potential energy, PE, along the PT coordinate is modeled as a pair of linearly coupled harmonic oscillators representing the N−H and O−H stretching motions of the normal and tautomeric forms.[27,62] We map the proton transfer along a coordinate defined by displacement from the equilibrium $S_1(N)$ position. On the basis of our calculations in section 3.3, we estimate the displacement from $S_1(N)$ to $S_1(T)$ to be 0.6 Å. The harmonic frequency is set to 2000 cm^{-1} for both motions, and the coupling is roughly estimated at 7500 cm^{-1} on the basis of the range reported for other proton-transfer systems.[61] The relatively strong coupling assumed in the model does result in a contraction of the distance between the minima of the two wells shown in Figures 8a and 9a from the initial displacement parameter of 0.6 Å. However, the resulting displacement remains within the accuracy of our estimation for this distance. The equilibrium energy difference from $S_1(N)$ to $S_1(T)$ in the absence of solvent stabilization is estimated from the static fluorescence ratios reported in cyclohexane[25] at −250 cm^{-1} for CAAQ and −700 cm^{-1} for TFAQ. We note that the parameters chosen for the model here differ significantly from those used by Neuwahl et al., where no explanation for the estimated values was presented.[27] The resulting PE curves along the PT are shown as the dash−dot−dash line in Figures 8a and 9a.

The solvation polarization energy is approximated with the Kirkwood−Onsager continuum solvation model as described in section 3.3 and shown in Table 5. The solvent coordinate is defined as the displacement from the solvent polarization energy of the ground-state normal form, $G_P - G_P[S_0(N)]$. Linear response is assumed along the solvent coordinate with a reorganization energy of 1500 cm^{-1} between $S_1(N)$ and $S_1(T)$. The resulting PE curves along this solvent coordinate are shown

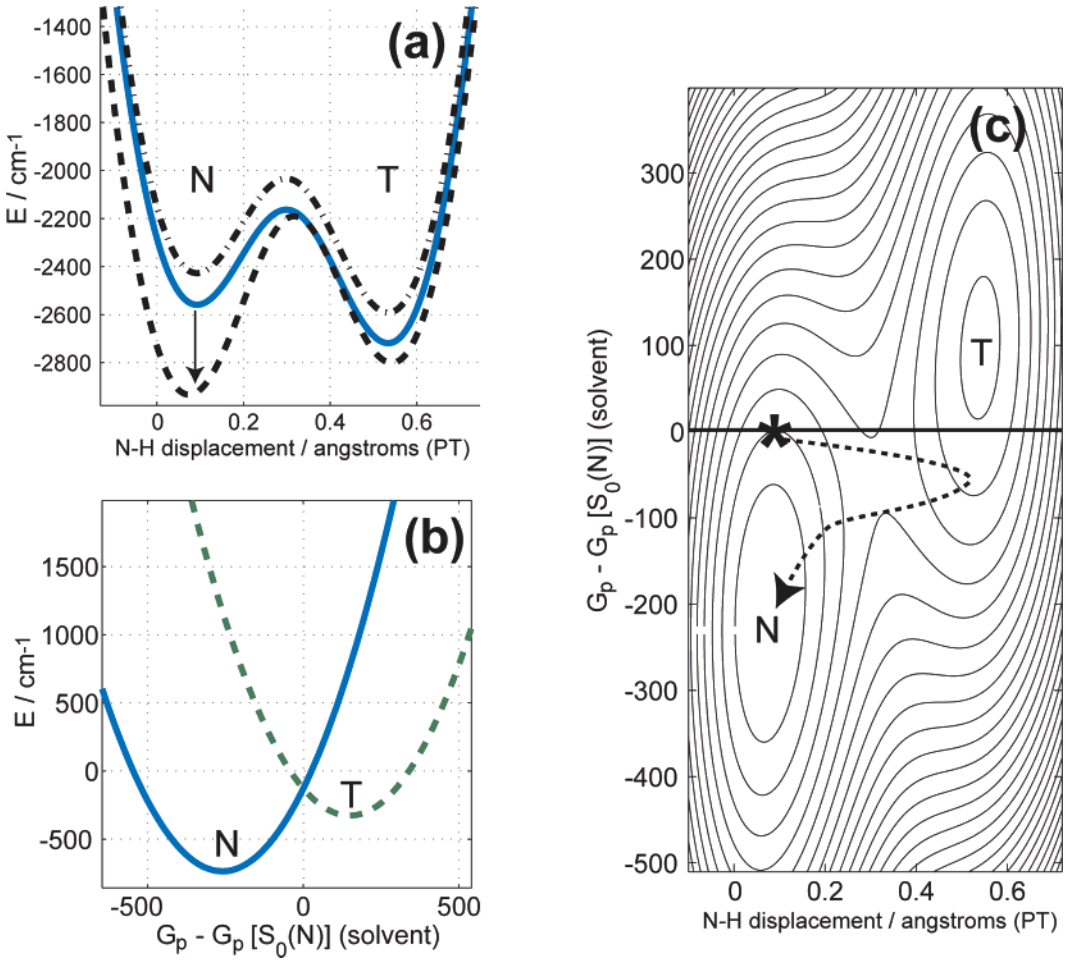

Figure 8. Illustration of the combined solvent and proton-transfer coordinates for CAAQ in acetonitrile. Details of the simple model employed are available in section 4.4. (a) The potential along the PT coordinate without the solvent model (· − · −), with the solvent model immediately after excitation from $S_0(N)$ (—), and assuming complete solvent relaxation at each point along the PT coordinate (- - -). (b) The solvent potentials for the excited-state normal (—) and tautomeric species (- - -). (c) The 2D excited-state PT surface, with the solid line indicating the point along the solvent coordinate that corresponds to $S_0(N)$.

in Figures 8b and 9b. Combining the models for the PT and solvent coordinates results in the 2D model shown for CAAQ and TFAQ in Figures 8c and 9c. These figures illustrate clearly that the energetics of the PT are strongly dependent on the position along the solvent coordinate. For both solutes, the PT is endothermic at the position along the solvent coordinate near the minimum of the normal form and exothermic near the minimum of the tautomeric form.

Our experimental results indicate a solvent-driven reversal in the displacement from PT equilibrium in the first 300 fs after excitation of CAAQ. The initial displacement along the solvent coordinate serves as the starting point when considering the effect of solvent reorganization in the excited-state reaction. The solvent configuration at $t = 0$ is determined by the equilibrium solvent configuration around $S_0(N)$. By defining the solvent coordinate relative to $S_0(N)$, this initial displacement is at zero and shown as the solid line in Figure 8c. The initial solvent displacement in the excited state is between the minimum for $S_1(N)$ and $S_1(T)$ and lies slightly closer to the $S_1(T)$ minimum. This results in a slightly exothermic profile along the PT coordinate at $t = 0$, the solid line in Figure 8a. In the model, PT initially favors $S_1(T)$ and involves a small barrier. In the limit of solvent equilibration at every point along the PT coordinate, the dashed line in Figure 8a, the reaction becomes endothermic. This is consistent with the experimental results, where initial progress along the PT coordinate is toward $S_1(T)$ and there is a subsequent reversal as the solvent reorganizes. The barrier creates a kinetic delay in the initial appearance of $S_1(T)$ on a similar time scale to inertial solvent reorganization (ca. 100 fs), and this translates to an initial concerted event where progress is along both coordinates in Figure 8c. At longer times, progress along the PT coordinate becomes fast compared to motion along the solvent coordinate and solvent reorganization is responsible for establishing the final equilibrium distribution. This type of trajectory is shown with a dashed line on Figure 8c and illustrates the ultrafast reversal of the initial increase in the $S_1(T)/S_1(N)$ ratio seen in our experiments on CAAQ.

The initial solvent configuration not only determines the energetic difference between $S_1(N)$ and $S_1(T)$ at $t = 0$ but it can also play a role in the effective barrier along the PT coordinate at $t = 0$. For TFAQ the initial ESIPT is ballistic, in contrast with the initial kinetic delay seen in CAAQ that has been attributed to a barrier along the PT coordinate.[27] In the pump−probe experiments of Neuwahl et al., the authors did not report results for TFAQ, but they did compare CAAQ with the ballistic PT exhibited in 1,8-dihydroxyanthraquinone (DHAQ). The authors explained the different dynamics observed in terms of structural differences in the molecules that shortened the distance along the PT coordinate in DHAQ, effectively eliminating the barrier. A similar explanation for loss of the barrier in TFAQ does not apply because there is very little difference in the structure of TFAQ and CAAQ at the site of PT, see section 3.3. However, consideration of the solvent reorganization

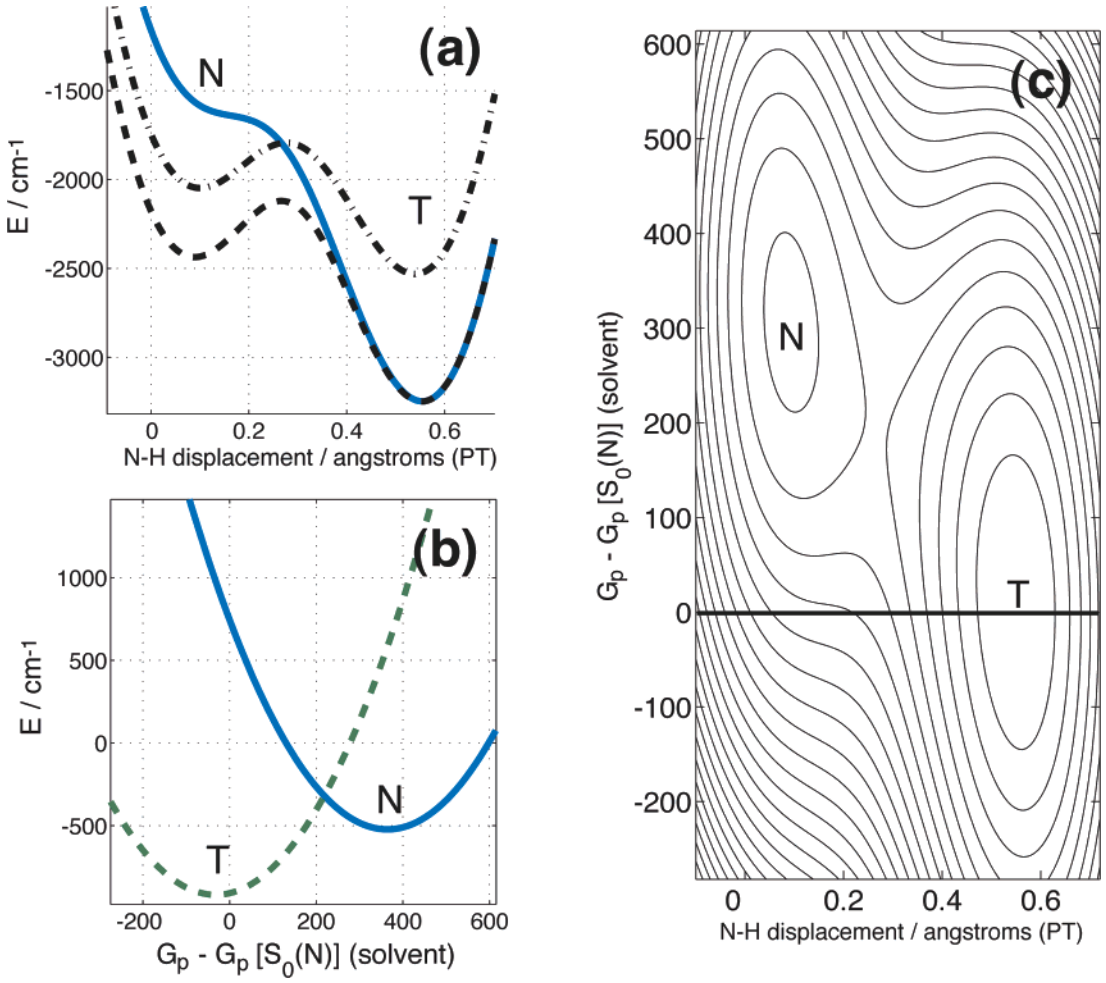

Figure 9. Illustration of the combined solvent and proton-transfer coordinates for TFAQ in acetonitrile. Details of the simple model employed are available in section 4.4. (a) The potential along the PT coordinate without the solvent model (· — · —), with the solvent model immediately after excitation from $S_0(N)$ (—), and assuming complete solvent relaxation at each point along the PT coordinate (- - -). (b) The solvent potentials for the excited-state normal (—) and tautomeric species (- - -). (c) The 2D excited-state PT surface, with the solid line indicating the point along the solvent coordinate that corresponds to $S_0(N)$.

coordinate can offer some insight. The additional driving force in TFAQ compared with CAAQ does lower the energy of $S_1(T)$ relative to $S_1(N)$. This causes a slight reduction, but not elimination of the forward barrier along the PT, see the dashed lines in Figure 9a. However, as shown by the solid line in Figure 9c, the initial solvent configuration for TFAQ determined by $S_0(N)$ is nearly identical to $S_1(T)$ and significantly displaced from $S_1(N)$. The result is that there is no barrier along the PT coordinate at the time of excitation, the solid line in Figure 9a. Although an increase in the coupling along the PT coordinate could also contribute to lowering the barrier, we believe that the initial solvent configuration plays an important part in the differences found for the initial ESIPT dynamics in AAQs.

4.5. τ-Dependence of the *t*-Slices. In this study, we have focused on RaPTORS *t*-slices taken with a τ delay near the peak of the inertial response. This was chosen for the large signal at this point and the sensitivity of this point in the response to both changes in the intermolecular solvent−solute interaction and the solvent kinetic energy.[30] However, by changing τ one can probe different portions of the intermolecular response. Recovering the complete intermolecular response (i.e., the full τ-dependence) as a function of *t* adds significant complexity to the experiments[30] and will be reported in a subsequent manuscript.[42] Here we compare the response at one later point along τ. This provides confirmation of the dynamics measured near the peak of the intermolecular response and indicates some subtle differences that arise when probing at a slightly later value of τ.

Figure 10 compares the fits for τ values near the peak of the TOR response and at a later fixed value of τ, 350 fs in acetonitrile and 360 fs in dichloromethane. The raw data, fits, and fitting parameters at the larger τ values are available in the Supporting Information. Although the data is shown with arbitrary scaling, the absolute signal intensities are reduced significantly as a result of a smaller TOR response at the longer τ delay. The fits at the two different τ values are very similar. This is consistent with the fact that the intermolecular spectrum consists of broad, overlapping time scales rather than well-resolved specific intermolecular motions. Increasing the τ delay by 200 fs may cause changes in the weighting of different contributions to the intermolecular response. However, at 350 or 360 fs the probe will still sample the same types of solvent motions, primarily inertial and translational, only at a slightly slower point in these distributions.

The fits do indicate small changes in the response at longer τ. For HPAQ, the initial negative response slows. For CAAQ, the initial rise is reduced prior to the turnaround in the response. Both of these results are consistent with the RaPTORS probe following changes in slower intermolecular motions at a later point in the TOR response. These slower motions have a reduced

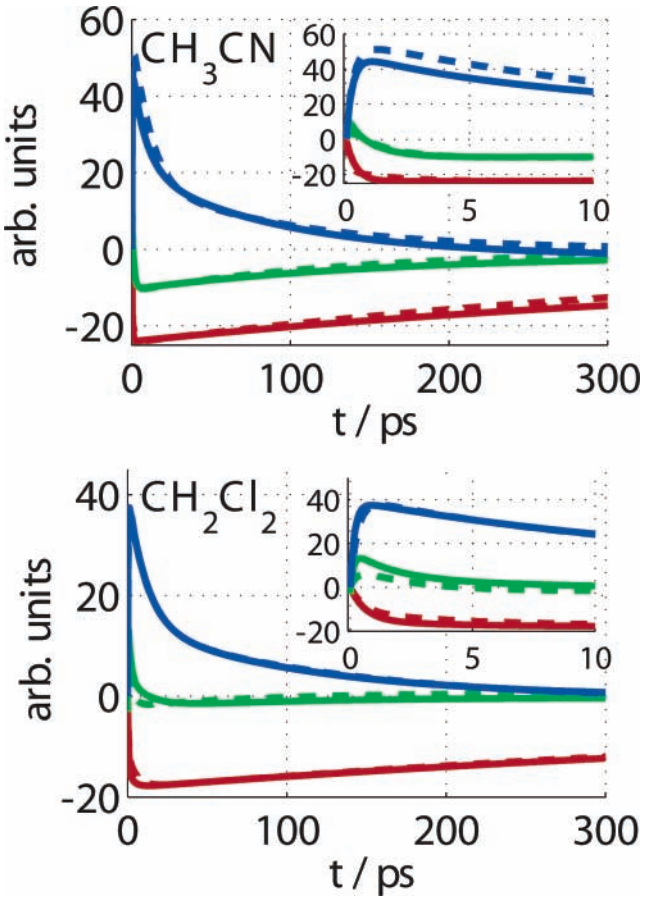

Figure 10. Comparison of the fits to *t*-slices at different values of τ, see text for details. In both plots, the red traces are for HPAQ, green traces are for CAAQ, and blue traces are for TFAQ. (top) The solvent is CH_3CN. Solid lines are fits at $\tau = 140$ fs, and dashed lines are fits at $\tau = 350$ fs. (bottom) The solvent is CH_2Cl_2. Solid lines are fits at $\tau = 180$ fs, and dashed lines are fits at $\tau = 360$ fs. For each AAQ, the fits at different τ values have been scaled to be equal at $t = 30$ ps.

sensitivity to the faster dynamics. There are also subtle changes in the TFAQ response times; however, the responses are generally very similar at the two reported values of τ. Probing over a much larger range of τ will be required to enhance the contrast between different contributions in the intermolecular solvent response associated with excited-state dynamics. Future determinations of the change in the entire TOR response will greatly broaden the range of different solvent motions being sampled, and should provide an improved understanding of how these different motions are affected by changes in the intermolecular solvent−solute interactions and changes in the solvent kinetic energy.

5. Conclusions

The work presented here represents the investigation of reactive systems through information gained from changes in the intermolecular solvent response. The RaPTORS method provides complementary information to techniques that probe changes in the solute during reactive events, resulting in a more complete picture of the complex dynamics that occur in the condensed phase. For the series of AAQs investigated in this study, the ability to follow changes in the intermolecular solvent−solute interaction leads to significant insight into the participation of the solvent as well as assignments of the changes in the solute. For example, in HPAQ where PT is restricted and CAAQ where PT is limited, the negative change measured with RaPTORS is a direct indication of an increase in the solvent−solute interaction upon excitation. This is consistent with the semiempirical calculations that indicated an increase in the dipole moment of both HPAQ and CAAQ; however, this is a reversal of previous assignments based on a negative solvatochromic shift. In the case of ESIPT in DCAQ and TFAQ, a rapid increase in the RaPTORS signal was shown to be the result of two important changes in the solvent associated with the reaction. In addition to a decrease of the intermolecular solvent−solute interaction in the excited state, there is also a rapid (ca. 200 fs) increase in the kinetic energy of the local solvent during ESIPT. The RaPTORS response follows the intermolecular transfer of energy from the local solvent as it dissipates into the bulk on a time scale of about 10 ps. Rapid changes in local solvent kinetic energy, which could be thought of in terms of the local nonequilibrium temperature during reactive events, are an important aspect of condensed phase dynamics that are not often considered and are not typically available from electronically resonant solute probes.

In the intermediate case of CAAQ, the measurements demonstrated a turn around in the displacement from equilibrium along the PT coordinate on the excited state within the first picosecond. This is a direct observation of the coupling between solvent reorganization and PT in the first (roughly) 200 fs after excitation. After the initial time scale, motion along PT coordinate becomes fast compared to the solvent, and the subsequent dynamics are controlled by solvent reorganization. Using a simple model, we are able to illustrate the influence of the solvent reorganization in these reactions and show how the initial solvent configuration at the time of excitation can have a significant influence on the reactive dynamics. This model offers an example of how the initial solvent configuration can account for the change from an observed kinetic delay in PT for CAAQ to a barrierless, ballistic event in TFAQ.

The work presented here offers an introduction to measuring changes in the intermolecular Raman response during reactive events in solution. Probing a single point in the TOR response illustrates the ability to probe these events from the perspective of the solvent, providing insight into the dynamic changes in the solvent−solute interaction and the rapidly changing local solvent kinetic energy. Future work to recover the changes in the entire intermolecular spectrum during reactive events should lead to even greater understanding of condensed-phase reactions.

Acknowledgment. We acknowledge the generosity of Professor Donald Truhlar, and Professor Christopher Cramer for providing us access to the locally developed MN-ZN program. Additionally, we acknowledge the Minnesota Supercomputing Institute for the allocation of time and resources on the supercomputer. This work was supported by NSF under award no. CHE-0211894. This work was supported in part by the MRSEC Program of the NSF under award no. DMR-0212302. D.B. thanks the Camille and Henry Dreyfus Foundation, the David and Lucile Packard Foundation, and 3M Company for their generous support. S.J.S. thanks the NSF for Fellowship support.

Supporting Information Available: AAQ static absorbance spectra, the measured heterodyne detected third-order Raman response for neat acetonitrile and dichloromethane, a detailed description of the solution to the series of consecutive steps used to fit the RaPTORS *t*-slices (eqs 4 and 5), fitting parameters for RaPTORS *t*-slices for all AAQs at $\tau = 350$ fs in acetonitrile and $\tau = 360$ fs in dichloromethane, and all raw RaPTORS *t* slices with fits for both acetonitrile and dichloromethane. This material is available free of charge via the Internet at http://pubs.acs.org.

References and Notes

(1) *Ultrafast Hydrogen Bonding Dynamics and Proton Transfer Prosesses in the Condensed Phase*, Vol. 23 of *Understanding Chemical Reactivity*; Elsaesser, T., Bakker, H. J., Eds.; Kluwer Academic Publishers: Boston, MA, 2002.

(2) *Proton Transfer in Hydrogen-Bonded Systems*, Vol. 291 of *NATO ASI Series B. Physics*; Bountis, T., Ed.; Plenum Press: New York, 1992.

(3) Jeffrey, G. A. *An Introduction to Hydrogen Bonding*; Oxford University Press: New York, 1997.

(4) Douhal, A.; Lahmani, F.; Zewail, A. H. *Chem. Phys.* **1996**, *207*, 477−498.

(5) Barbara, P.f.; Walker, G. C.; Smith, T. P. *Science* **1992**, *256*, 975−981.

(6) Voth, G. A.; Hochstrasser, R. M. *J. Phys. Chem.* **1996**, *100*, 13034−13049.

(7) Taylor, C. A.; El-Bayoumi, M. A.; Kasha, M. *Proc. Natl. Acad. Sci. U.S.A.* **1969**, *63*, 253−260.

(8) Lowdin, P. O. *Rev. Mod. Phys.* **1963**, *35*, 724−732; discussion 732−733.

(9) Ingham, K. C.; Abu-Elgheit, M.; El-Bayoumi, M. A. *J. Am. Chem. Soc.* **1971**, *93*, 5023−5025.

(10) Ingham, K. C.; El-Bayoumi, M. A. *J. Am. Chem. Soc.* **1974**, *96*, 1674−1682.

(11) Chen, Y.; Gai, F.; Petrich, J. W. *J. Am. Chem. Soc.* **1993**, *115*, 10158−10166.

(12) Chou, P.-T.; Yu, W.-S.; Chen, Y.-C.; Wei, C.-Y.; Martinez, S. *J. Am. Chem. Soc.* **1998**, *120*, 12927−12934.

(13) Waluk, J.; Bulska, H.; Pakula, B.; Sepiol, J. *J. Lumin.* **1981**, *24*−*25*, 519−522.

(14) Herbich, J.; Sepiol, J.; Waluk, J. *J. Mol. Struct.* **1984**, *114*, 329−332.

(15) McMorrow, D.; Aartsma, T. J. *Chem. Phys. Lett.* **1986**, *125*, 581−585.

(16) Moog, R. S.; Maroncelli, M. *J. Phys. Chem.* **1991**, *95*, 10359−10369.

(17) Gai, F.; Chen, Y.; Petrich, J. W. *J. Am. Chem. Soc.* **1992**, *114*, 8343−8345.

(18) Fernandez-Ramos, A.; Smedarchina, Z.; Siebrand, W.; Zgierski, M. Z. *J. Chem. Phys.* **2001**, *114*, 7518−7526.

(19) Herbich, J.; Waluk, J.; Thummel, R.; Hung, C.-Y. *J. Photochem. Photobiol., A* **1994**, *80*, 157−160.

(20) Kyrychenko, A.; Stepanenko, Y.; Waluk, J. *J. Phys. Chem. A* **2000**, *104*, 9542−9555.

(21) Thummel, R. P.; Hung, C.-Y.; Hoepfner, T.; Russel, J. *J. Chem. Soc., Chem. Commun.* **1994**, *7*, 857−858.

(22) Fiebig, T.; Chachisvilis, M.; Manger, M.; Zewail, A. H.; Douhal, A.; Garcia-Ochoa, I.; de La Hoz Ayuso, A. *J. Phys. Chem. A* **1999**, *103*, 7419−7431.

(23) Flom, S. R.; Barbara, P. F. *J. Chem. Phys.* **1985**, *89*, 4489−4494.

(24) Barbara, P. F.; Jarzeba, W. *Adv. Photochem.* **1990**, *15*, 1−68.

(25) Smith, T. P.; Zaklika, K. A.; Thakur, K.; Walker, G. C.; Tominaga, K.; Barbara, P. F. *J. Phys. Chem.* **1991**, *95*, 10465−10475.

(26) Smith, T. P.; Zaklika, K.; Thakur, K. A.; Barbara, P. F. *J. Am. Chem. Soc.* **1991**, *113*, 4035−4036.

(27) Neuwahl, F. V. R.; Bussotti, L.; Righini, R.; Buntinx, G. *Phys. Chem. Chem. Phys.* **2001**, *3*, 1277−1283.

(28) Nagaoka, S.; Yamamoto, S.; Mukai, K. *J. Photochem. Photobiol., A* **1997**, *105*, 29−33.

(29) Underwood, D. F.; Blank, D. A. *J. Phys. Chem. A* **2003**, *107*, 956−961. Underwood, D. F.; Blank, D. A. *J. Phys. Chem. A* **2003**, *107*, 9736.

(30) Underwood, D. F.; Blank, D. A. *J. Phys. Chem. A* **2005**, *109*, 3295−3306.

(31) Schmidtke, S. J.; Underwood, D. F.; Blank, D. A. *J. Am. Chem. Soc.* **2004**, *126*, 8620−8621.

(32) Desai, R. D.; Desai, R. N. *J. Indian Chem. Soc.* **1956**, *33*, 559−560.

(33) Bayer & Co., D. R. P. 213960, **1909**, *2*, 1286.

(34) Vigorita, M. G.; Previtera, T.; Trovato, A.; Monforte, M. T.; Barbera, R.; Bisignano, G. *Farmaco* **1989**, *44*, 173−184.

(35) Molecular Probes, Inc. Molecular Dye Sampler Kit (R-14782) Product Information and refences therein. www.probes.com.

(36) Mukamel, S. *Principles of Nonlinear Optical Spectroscopy*; Oxford University Press: New York, 1995.

(37) McMorrow, D.; Lotshaw, W. T. *J. Phys. Chem.* **1991**, *95*, 10395−10406.

(38) Fleming, G. A.; Passino, S. A.; Nagasawa, Y. *Philos. Trans. R. Soc. London, Ser. A* **1998**, *356*, 389−404.

(39) Maroncelli, M.; Kumar, V. P.; Papazyan, A. *J. Phys. Chem.* **1993**, *97*, 13−17.

(40) Farrer, R. A.; Loughnane, B. J.; Deschenes, L. A.; Fourkas, J. T. *J. Chem. Phys.* **1997**, *106*, 6901−6915.

(41) Park, S.; Flanders, B. N.; Shang, X.; Westervelt, R. A.; Kim, J.; Scherer, N. F. *J. Chem. Phys.* **2003**, *118*, 3917−3920.

(42) Schmidtke, S. J.; Underwood, D. F.; Blank, D. A., to be submitted for publication.

(43) Etchepare, J.; Grillon, G.; Chambaret, J. P.; Hamoniaux, G.; Orszag, A. *Opt. Commun.* **1987**, *63*, 329−334.

(44) Hellwarth, R. W. *Prog. Quantum Electron.* **1977**, *5*, 1−68.

(45) Frisch, M. J.; Trucks, G. W.; Schlegel, H. B.; Scuseria, G. E.; Robb, M. A.; Cheeseman, J. R.; Zakrzewski, V. G.; Montgomery, J. A., Jr.; Stratmann, R. E.; Burant, J. C.; Dapprich, S.; Millam, J. M.; Daniels, A. D.; Kudin, K. N.; Strain, M. C.; Farkas, O.; Tomasi, J.; Barone, V.; Cossi, M.; Cammi, R.; Mennucci, B.; Pomelli, C.; Adamo, C.; Clifford, S.; Ochterski, J.; Petersson, G. A.; Ayala, P. Y.; Cui, Q.; Morokuma, K.; Malick, D. K.; Rabuck, A. D.; Raghavachari, K.; Foresman, J. B.; Cioslowski, J.; Ortiz, J. V.; Stefanov, B. B.; Liu, G.; Liashenko, A.; Piskorz, P.; Komaromi, I.; Gomperts, R.; Martin, R. L.; Fox, D. J.; Keith, T.; Al-Laham, M. A.; Peng, C. Y.; Nanayakkara, A.; Gonzalez, C.; Challacombe, M.; Gill, P. M. W.; Johnson, B. G.; Chen, W.; Wong, M. W.; Andres, J. L.; Head-Gordon, M.; Replogle, E. S.; Pople, J. A. *Gaussian 98*, revision A.11; Gaussian, Inc.: Pittsburgh, PA, 1998.

(46) Lee, C.; Yang, W.; Parr, R. G. *Phys. Rev. B: Condens. Matter Mater. Phys.* **1988**, *37*, 785−789.

(47) Miehlich, B.; Savin, A.; Stoll, H.; Preuss, H. *Chem. Phys. Lett.* **1989**, *157*, 200−206.

(48) Becke, A. D. *J. Chem. Phys.* **1993**, *98*, 5648−5652.

(49) Easton, R. E.; Giesen, D. J.; Welch, A.; Cramer, C. J.; Truhlar, D. G. *Theor. Chim. Acta* **1996**, *93*, 281−301.

(50) Zerner, M. C.; Ridley, J. E.; Bacon, A. D.; Head, J. D.; Edwards, W. D.; Head, J. D.; McKelvey, J.; Cuberson, J. C.; Knappe, P.; Cory, M. G.; Weiner, B.; Baker, J. D.; Parkinson, W. A.; Kannis, D.; Yu, J.; Roesch, N.; Kotzian, M.; Tamm, T.; Karelson, M. M.; Zheng, X.; Pearl, G.; Broo, A.; Albert, K.; Cullen, J. M.; Li, J.; Hawkins, G. D.; Thompson, J. D.; Liotard, D. A.; Cramer, C. J.; Truhlar, D. G. *ZINDO-MN*, version 1.1; Quantum Theory and Project, University of Florida, Gainesville, and Department of Chemistry, University of Minnesota, Minneapolis, MN, 2002.

(51) Li, J.; Williams, B.; Cramer, C. J.; Truhlar, D. G. *J. Chem. Phys.* **1999**, *110*, 724−733.

(52) Li, J.; Cramer, C. J.; Truhlar, D. G. *Int. J. Quantum Chem.* **2000**, *77*, 264−280.

(53) Winget, P.; Dolney, D.; Giesen, D.; Cramer, C. J.; Truhlar, D. G. Supercomputer Institute, University of Minnesota, Minnesota solvent descriptor database.

(54) Horng, M. L.; Gardecki, J. A.; Maroncelli, M. *J. Phys. Chem. A* **1997**, *101*, 1030−1047.

(55) Kiprianov, A. *Russ. Chem. Rev.* **1960**, *29*, 618−626.

(56) Cramer, C. J. *Essentials of Computational Chemistry: Theories and Models*, 2nd ed.; John Wiley & Sons: Hoboken, NJ, 2004.

(57) Kirkwood, J. G. *J. Chem. Phys.* **1934**, *2*, 351−361.

(58) Onsager, L. *J. Am. Chem. Soc.* **1936**, *58*, 1486−1493.

(59) Horng, M. L.; Gardecki, J. A.; Papazyan, A.; Maroncelli, M. *J. Phys. Chem.* **1995**, *99*, 17311−17337.

(60) Maroncelli, M. *J. Chem. Phys.* **1991**, *94*, 2084−2103.

(61) Kiefer, P. M.; Hynes, J. T. *J. Phys. Chem. A.* **2002**, *106*, 1834−1849.

(62) Arthen-Engeland, T.; Bultmann, R.; Ernsting, N. P.; Rodriguez, M. A.; Thiel, W. *Chem. Phys.* **1997**, *163*, 43−53.